

Kontrolle rauschinduzierter Oszillationen im Van-der-Pol Modell

Analyt. Näherung der spektralen Leistungsdichte:

Fourier-Transform des mean-field-gew. $\dot{x} = y$
 $\dot{y} = \tilde{\epsilon} y - \omega_0^2 x + D \xi(t) + K [y(t-\tau) - y(t)]$

$$x(t) = \int_{-\infty}^{\infty} d\omega e^{-i\omega t} \hat{x}(\omega)$$

$$-i\omega \hat{x}(\omega) = \hat{y}(\omega)$$

$$-i\omega \hat{y}(\omega) = \tilde{\epsilon} \hat{y}(\omega) - \omega_0^2 \hat{x}(\omega) + D \hat{\xi}(\omega) + K \hat{y}(\omega) (e^{i\omega\tau} - 1)$$

Elim. von $\hat{x}(\omega) = \frac{i}{\omega} \hat{y}(\omega)$:

$$-i\omega \hat{y} - \tilde{\epsilon} \hat{y} + i \frac{\omega_0^2}{\omega} \hat{y} - K (e^{i\omega\tau} - 1) \hat{y} = D \hat{\xi} \quad | \cdot i\omega$$

$$\hat{y}(\omega) = \frac{i\omega D \hat{\xi}(\omega)}{\omega^2 - \omega_0^2 - i\omega \tilde{\epsilon} - i\omega K (e^{i\omega\tau} - 1)}$$

$$\langle \hat{y}(\omega) \hat{y}^*(\omega') \rangle = \frac{(i\omega D)(-i\omega' D) \langle \hat{\xi}(\omega) \hat{\xi}^*(\omega') \rangle}{(\omega^2 - \omega_0^2 - i\omega [\tilde{\epsilon} + K(e^{i\omega\tau} - 1))](\omega'^2 - \omega_0^2 + i\omega' [\tilde{\epsilon} + K(e^{-i\omega'\tau} - 1)])}$$

$$\langle \hat{\xi}(\omega) \hat{\xi}^*(\omega') \rangle = \frac{1}{(2\sigma)^2} \int_{-\infty}^{\infty} dt e^{i\omega t} \int_{-\infty}^{\infty} dt' e^{-i\omega' t'} \underbrace{\langle \xi(t) \xi(t') \rangle}_{\delta(t-t')}$$

$$= \frac{1}{2\pi} \underbrace{\frac{1}{2\pi} \int_{-\infty}^{\infty} dt e^{i(\omega - \omega')t}}_{\delta(\omega - \omega')}$$

$$\omega = \omega' \Rightarrow \langle \hat{y}(\omega) \hat{y}^*(\omega') \rangle = \frac{D^2}{2\pi} \frac{\omega^2 \delta(\omega - \omega')}{(\omega^2 - \omega_0^2 + \omega K \sin \omega\tau)^2 + \omega^2 (\tilde{\epsilon} - K(1 - \cos \omega\tau))^2}$$

Wiener - Khinchine - Theorem:

$$\begin{aligned} \langle \hat{y}(\omega) \hat{y}^*(\omega') \rangle &= \frac{1}{(2\pi)^2} \int_{-\infty}^{\infty} dt e^{i\omega t} \int_{-\infty}^{\infty} dt' e^{-i\omega' t'} \langle y(t) y(t') \rangle \\ &= \frac{1}{2\pi} \int_{-\infty}^{\infty} dt e^{i(\omega - \omega')t} \underbrace{\frac{1}{2\pi} \int_{-\infty}^{\infty} ds e^{i\omega'(t-t') - i\omega' s}}_{S(\omega')} \langle y(t) y(t+s) \rangle \\ &\quad \underbrace{\hspace{10em}}_{S(\omega - \omega')} \end{aligned}$$

$$\Rightarrow S_{yy}(\omega) = \frac{D^2}{2\pi} \frac{\omega^2}{(\omega^2 - \omega_0^2 + \omega K \sin \omega \tau)^2 + \omega^2 (\tilde{\epsilon} - K(1 - \cos \omega \tau))^2}$$

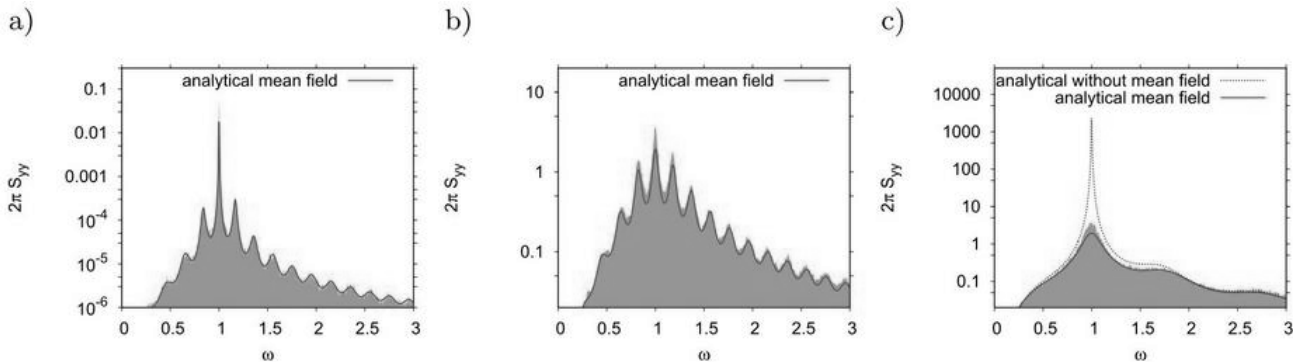
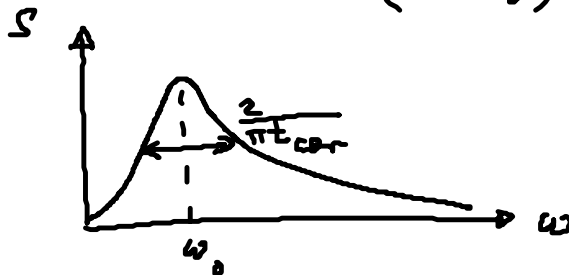


Fig. 4 - Spectrum $S_{yy}(\omega)$ for the VdP system in the presence of delayed feedback for $\epsilon = -0.01$, $K = 0.2$: a) $D = 0.003$, $\tau = 31.4$; b) $D = 0.5$, $\tau = 31.4$; c) $D = 0.5$, $\tau = 6.3$. Shaded: numerically simulated spectra; solid line: spectrum estimated analytically by (19); dashed line in c): spectrum estimated analytically without mean field ($\tilde{\epsilon} = \epsilon$) [14].

Pomplun et al, Ewophys. Lett. 2005

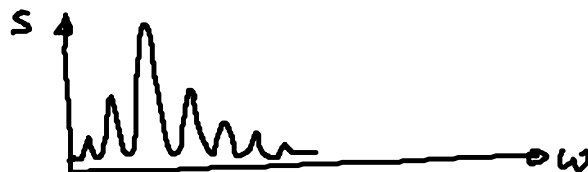
herausragende Übereinstimmung der mean-field-Näherung mit der vollen nichtlin. Simul. der Dgl., sogar für große D

$$K=0 : S(\omega) = \frac{D^2}{2\pi} \frac{\omega^2}{(\omega^2 - \omega_0^2)^2 + \omega^2 \tilde{\epsilon}^2}$$



Lorentzkurve mit Max. bei ω_0 u. Halbwertsbreite $\approx \frac{|\tilde{\epsilon}|^2}{2} = \frac{2}{\pi t_{cor}}$

$K \neq 0$: immer mehr Nebenmax. mit zunehmendem τ



Generisches Modell für Anregbarkeit Typ I

(knapp unterhalb der SNIPER-Bifurkation)

Aust, Hövel, Hizanidis, Schöll, Eur. Phys. J - ST 187, 77 (2010)

$$\begin{aligned} \dot{x} &= x(1-x^2-y^2) + y(x-b) + D\xi(t) + K[x(t-\tau) - x(t)] \\ \dot{y} &= y(1-x^2-y^2) - x(x-b) + D\xi(t) + K[y(t-\tau) - y(t)] \end{aligned}$$

$K=D=0$ $b < 1$: stab. Fixp. (Knoten), anregbares Regime
 $b = 1$: Sattel-Knoten-Bif. auf Grenzzyklus $r=1$, $T \rightarrow \infty$

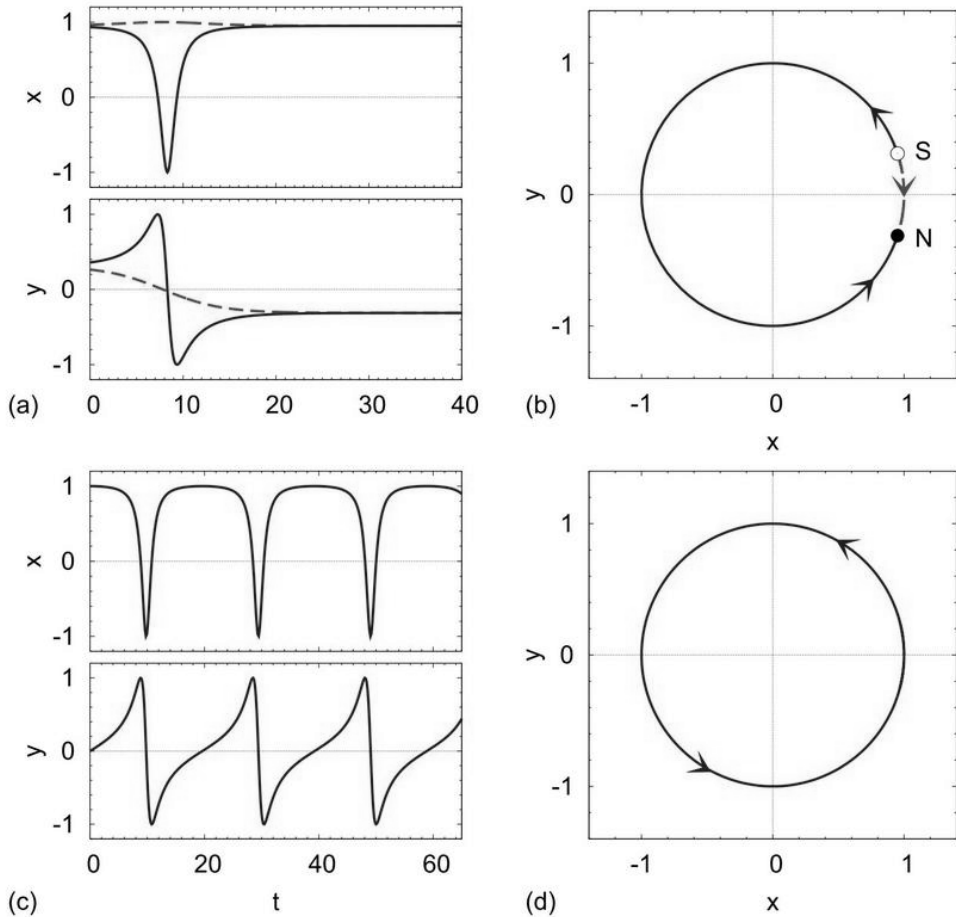
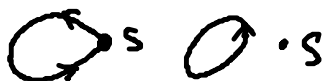


Fig. 1. (Color online) Time series (a),(c) and phase portraits (b),(d) of the analytic solutions of Eqs. (2). Panels (a),(b) refer to $b = 0.95 < 1$ with analytic solutions given by Eq. (7); full (blue) and broken (red) lines refer to two different initial conditions. Panels (c),(d) correspond to $b = 1.05 > 1$, see Eq. (8). ($K = D = 0$)

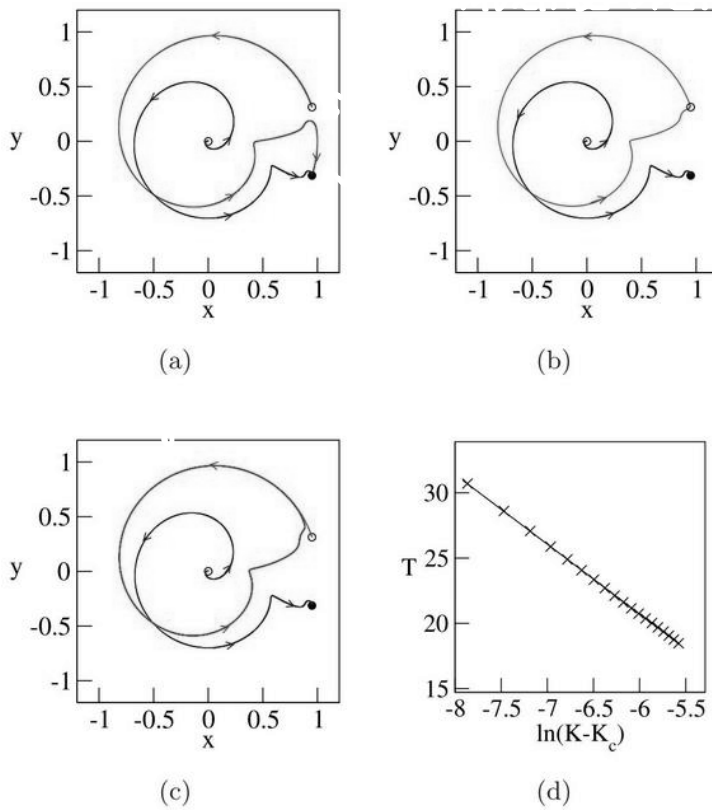
$D=0$: Delay-induzierte globale (homokline) Bifurk.

Hizanidis et al., Int. J. Bif. Chaos 18, 1759 (2008)

Fixp. N (node) bleibt stabil, aber homokline Bif. eines stab. Grenzzyklus $r > 0$, $T \rightarrow \infty$

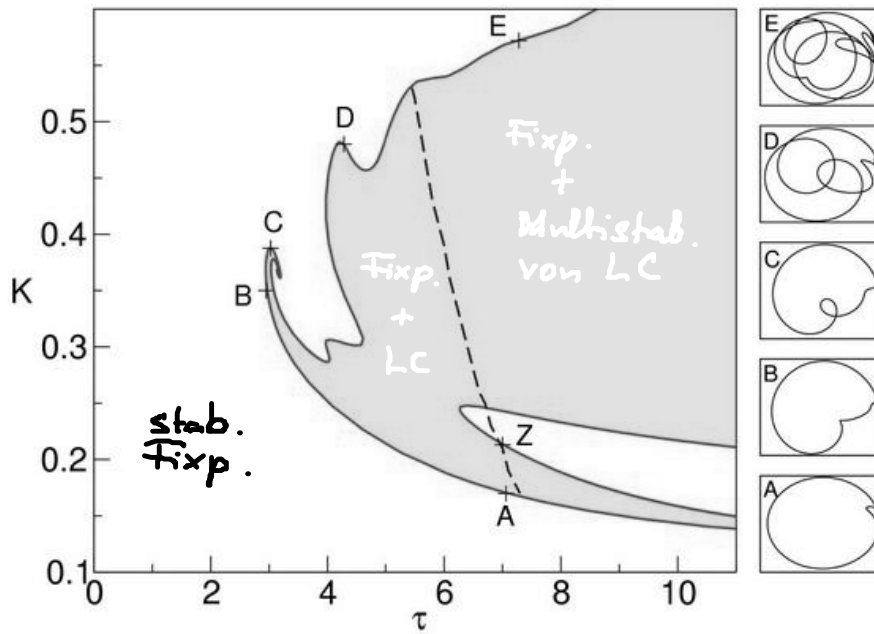


im Bif. plot.



Periode $T \sim \ln|K-K_c|$

Fig. 2. (a) Two-dimensional projection of the phase space below the homoclinic bifurcation ($K = 0.335$). (b) Homoclinic orbit (red) achieved at $K_c = 0.3401$. (c) Delay-induced limit cycle (red) above the homoclinic bifurcation ($K = 0.3438$). (d) Scaling of the oscillation period T above but close to the critical point K_c (crosses: simulation data, solid line: linear fit). Full and open circles mark stable and unstable fixed points, respectively. Parameters: $b = 0.95$, $\tau = 3$.



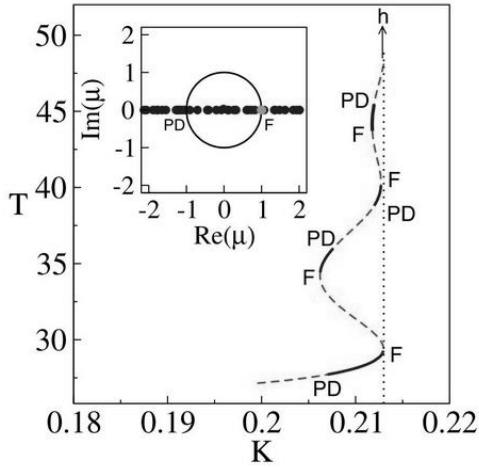
Bif. diagrams
($D=0$)

Shilnikov-Theorie
saddle quantity
 $\sigma_0 = \text{Re} \lambda_s + \text{Re} \lambda_u$

Fig. 2. Curve of homoclinic bifurcations (red) in the K - τ plane.

Fig. 3. Curve of homoclinic bifurcations (red) in the $K-\tau$ plane (left). A-E labels various points with homoclinic orbits, which are shown in the $x-y$ phase plane in the panel on the right. Delay-induced limit cycles exist, in addition to the stable fixed point, in the yellow area. The blue dashed curve separates the regions $\sigma_0 < 0$ (left) and $\sigma_0 > 0$ (right).

↑
 führender stab./instab.
 Eigenwert des
 Sattel-Fokus



(b)

Fig. 5. (a) Period T of limit cycle born in a homoclinic bifurcation at $(K, \tau) = (0.17145, 7)$ (point A in Fig. 3, $\sigma_0 < 0$). (b) Period T of limit cycles in the multistable regime at $(K, \tau) = (0.213, 7)$ (point Z in Fig. 3, $\sigma_0 > 0$), undergoing infinitely many fold (F) and period-doubling (PD) bifurcations, before ending in a homoclinic orbit h for $T \rightarrow \infty$ at $K = 0.213$. Solid blue and red dashed lines denote stable and unstable limit cycles, respectively. The insets show the two leading Floquet multipliers of the periodic orbit $\mu_1 = 1$ (green) and μ_2 (blue) with K as a parameter in (a), and T as a parameter in (b), in the complex plane $b = 0.95$.

$D \neq 0$: Kontrolle rauschinduzierter + rauschbeeinflusster
 Oszillationen

↓
 delay-induzierte
 determinist. Grenzzyklen

- Kohärenzresonanz (für $K=0$) wird verstärkt durch zeitverzögerte Rückkopplungskontrolle

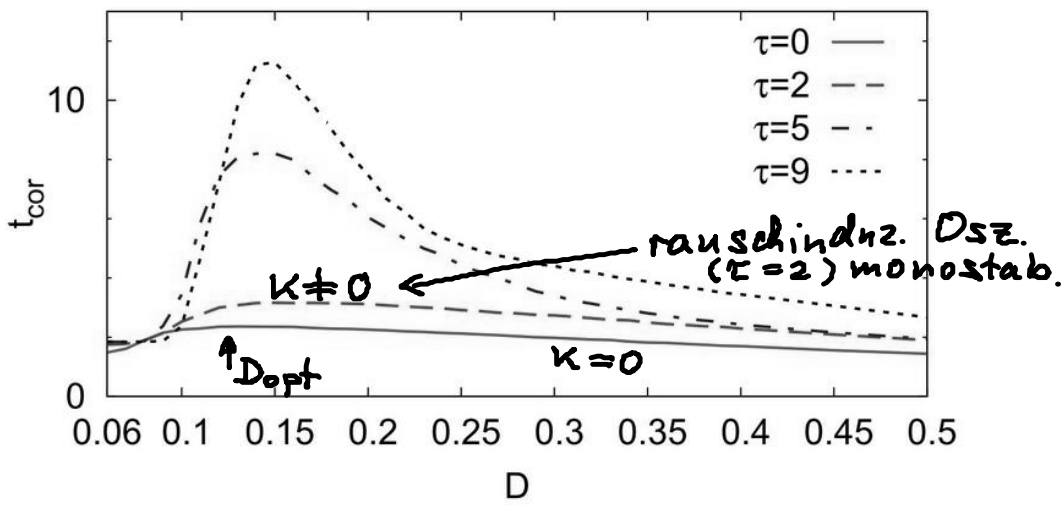


Fig. 4. (Color online) Correlation time in dependence on the noise intensity D for different time delays τ . The solid (green) curve corresponds to the uncontrolled system ($\tau = 0$). The dashed (red), dash-dotted (blue), and dotted (black) curves refer to values of $\tau = 2, 5$, and 9 , respectively. Other parameters: $b = 0.95$ and $K = 0.25$.

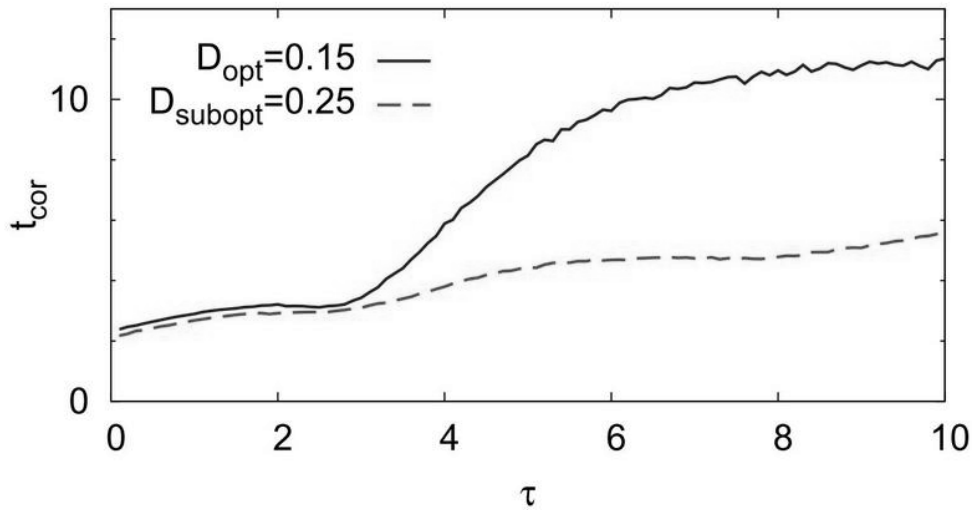


Fig. 5. (Color online) Correlation time t_{cor} in dependence on the time delay τ for two values of the noise intensity D . The dashed (red) curve corresponds to $D_{subopt} = 0.25$ and the solid (blue) curve refers to $D_{opt} = 0.15$. Other parameters: $b = 0.95$ and $K = 0.25$.

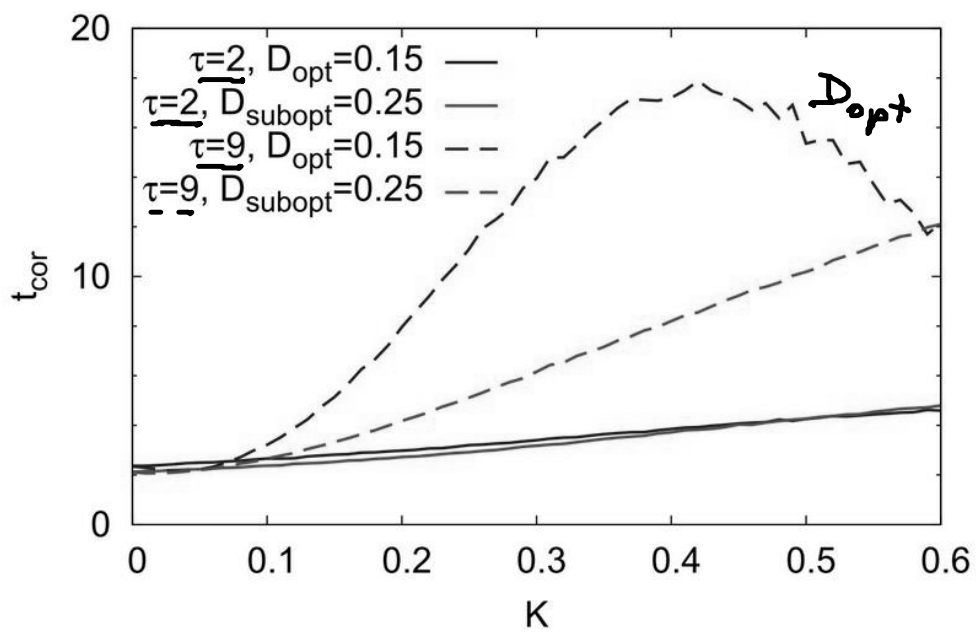


Fig. 6. (Color online) Correlation time t_{cor} in dependence on the control strength K for two values of the noise intensity D and two values of the delay time τ . The gray (red) and black (blue) curves depict the cases of D_{subopt} and D_{opt} , respectively. The solid and dashed lines correspond to $\tau = 2$ and $\tau = 9$, respectively. Other parameter: $b = 0.95$.